RECOVERING THE PASSIVE PROPERTIES OF TAPERED DENDRITES FROM SINGLE AND DUAL POTENTIAL RECORDINGS

Steven J. Cox

Department of Computational and Applied Mathematics
MS 134, Rice University, 6100 Main St., Houston, TX 77005
cox@rice.edu, phone: 713-348-5192, fax: 713-348-5318

Abstract: We demonstrate that measurement of the membrane potential at one or more sites on a branched and tapered neuron following a known transient injection of subthreshold somatic current uniquely determines the cell's passive electrical properties. That is, knowledge of the potentials allows recovery of the cell's axial resistance, membrane capacitance, membrane conductance and soma conductance. The argument underlying uniqueness leads immediately to a constructive, robust algorithm that we successfully test on synthetic data. The robustness stems from the fact that the algorithm requires only a few weighted integrals, or moments, of the measured potentials.

Keywords: Moment methods, integrals of transients, eigenfunction expansions, finite element method.

1. Introduction

To quantify, at the cellular level, a neuron's ability to integrate synaptic input one must determine the neuron's shape and electrical characteristics. Determination of shape, at least in vitro, is straightforward, though tedious, via staining, light microscopy and commercially available imaging software, see e.g., N.J. Bannister & J. Larkman [1]. Determination of electrical characteristics is significantly more challenging. The desired characteristics are the cell's **passive** properties; axial resistance, R_a, membrane capacitance, C_m, membrane conductance, G_m, and soma conductance, G_s, and **active** properties; location, conductance and kinetics of a variety of ion channels. The experimental data from which the determination is to be made is not particularly rich, namely voltage transient(s) recorded at one (or more) dendritic location(s) following a specified injection of current. With regard to determining passive properties, Rall developed and championed "peeling" methods for single fibers (or neurons equivalent to such) and "constrained optimization" methods coupled with compartmental models for more general neurons, see Rall *et al.* [2] and Vanier & Bower [3]. While Rall's methods make explicit use of pointwise values of the voltage transients Cox [4] introduced and extended, Cox & Ji [5],[6] and Cox & Griffith [7], an alternative approach that relies on only a few weighted integrals of these transients. Similar techniques were employed by Engelhardt *et al.* [8] as an application of a result of Eisenberg & Mathias [9], itself an elaboration of a technique first established in the appendix, with W.K. Chandler, of Adrian & Almers' [10] work on frog muscle. It is unfortunate that the enthusiastic reception

> "The fundamental idea introduced by Adrian *et al.*, which we feel deserves the name breakthrough, is the computation of an integral of the transient response of a prepa-

ration and the evaluation of that integral in terms of properties of theoretical models of the preparation, usually an equivalent circuit with a structural interpretation."

by Eisenberg & Mathias [9,§H] did not lead to widespread adoption and application of their idea. In particular, its absence from the text of Jack *et al.* [11] and the excellent and influential surveys of Rall [12],[13] and Rall & Agmon–Snir [14] is notable, especially as the latter incorporates Agmon–Snir's [15] work on integrals of transients! This is an important instance of work on muscle failing to fully inform work on nerve even though Eisenberg & Mathias recognized that the work of Adrian *et al.* transcended cell type and there were many thinkers, e.g., A.L. Hodgkin, who contributed equally to muscle and nerve. In fact the quote above is an echo of Hodgkin's remark, [16], that E.D. Adrian (the father of R.H.) "made what in the jargon of today (which Adrian detested) would be called a break-through".

The aim of the present work is to extend the 'integrals of transients' method of Adrian *et al.* [10] to the recovery of the passive properties of cells that branch and taper. We do this in steps, beginning in §2 with a tapered soma less fiber. We append a soma in §3 and permit arbitrary branching in §4. The extension from uniform to tapered structures is effected by a splitting of observed potentials into constitutive and anatomical components. More precisely, we accommodate spatial nonuniformity by expanding the voltage response in a series of eigenfunctions that encode the cell's morphology but are independent of its (unknown) electrical constitution. This expansion, and the aforementioned splitting permit us to reduce the search for four passive parameters to solving two scalar equations, $H(q) = H_0$ and $P(\gamma) = P_0$ where $q = 2R_aG_m$, $\gamma = 2R_a(G_m - G_s)$, H_0 and P_0 are explicit combinations of moments of the measured potentials and the functions H and P depend only on eigendata extracted from the cell's geometry. We derive and solve these equations for several model cells and show the solutions to be tolerant of modest levels of noise in the measured geometry and potentials.

The finite element method provides a convenient methodology for capturing taper and is superior to finite differences, see Fix and Strang [17], in the approximation of eigenvalues. We therefore adopt it in our recovery algorithm and numerical simulations. As such methods have received little attention in the neuroscience literature we devote an appendix to the construction of the underlying finite linear systems.

2. **The Tapered Fiber**

Following Rall [18], we consider a fiber of length ℓ and radius $a(x)$ at the point x. We denote by $v(x,t)$ the difference from rest of the membrane potential at point x and time t. The difference in v along the fiber is proportional to the axial current, i, via

$$v_x(x,t) = -\frac{R_a}{\pi a^2(x)} i(x,t) \tag{2.1}$$

where R_a is the axial resistance in $k\Omega\, cm$. Balancing axial and membrane currents then produces

$$i_x(x,t) = -2\pi a(x)\sqrt{1+(a'(x))^2}(C_m v_t(x,t) - G_m v(x,t)) \tag{2.2}$$

where C_m is the membrane capacitance ($\mu F/cm^2$), and G_m is the membrane conductance (mS/cm^2). Solving (2.1) for i, differentiating with respect to x and then substitution into (2.2) yields

$$\frac{1}{2R_a}(a^2 v_x)_x = a\sqrt{1+(a')^2}(C_m v_t + G_m v). \tag{2.3}$$

We assume that the fiber is initially at rest

$$v(x,0) = 0, \quad 0 < x < \ell, \tag{2.4}$$

that it receives a current stimulus, i_0, at the left

$$v_x(0,t) = -\frac{R_a}{\pi a^2(0)} i_0(t), \quad 0 < t, \tag{2.5}$$

and is sealed at the right

$$v_x(\ell,t) = 0, \quad 0 < t. \tag{2.6}$$

As a varies with x we may not, except in a few special cases, represent v in terms of elementary functions. The key to our approach then, is to represent it in terms of eigenfunctions that incorporate the taper a but are independent of the fiber's electrical properties. More precisely, we write

$$v(x,t) = \sum_{n=0}^{\infty} \psi_n(t)\phi_n(x) \tag{2.7}$$

where the ϕ_n satisfy

$$-(a^2\phi_n')' = \mu_n a\sqrt{1+(a')^2}\phi_n, \quad 0 < x < \ell, \tag{2.8}$$

$$\phi_n'(0) = \phi_n'(\ell) = 0. \tag{2.9}$$

Each eigenvalue is simple and nonnegative and so we order them like

$$0 = \mu_0 < \mu_1 < \mu_2 < \cdots \tag{2.10}$$

As the operator on the left in (2.8), subject to (2.9), is selfadjoint we may conclude that the eigenfunctions are orthonormal with respect to the natural inner product,

$$\int_0^\ell a\sqrt{1+(a')^2}\phi_n\phi_m\,dx = \delta_{mn} \equiv \begin{cases} 1 & \text{if } m = n, \\ 0 & \text{if } m \neq n. \end{cases} \tag{2.11}$$

This orthonormality permits us to multiply each side of (2.7) by $a\sqrt{1+(a')^2}\phi_m$ and integrate and find

$$\psi_n(t) = \int_0^\ell a(x)\sqrt{1+(a')^2}v(x,t)\phi_n(x)\,dx, \tag{2.12}$$

an implicit (in the sense that it depends on the unknown v) equation for ψ_n. We now differentiate throughout with respect to t and arrive (thanks to (2.3)–(2.6)) at a simple, explicit, ordinary differential equation for ψ_n.

$$\begin{aligned}
\psi_n'(t) &= \int_0^\ell a(x)\sqrt{1+(a')^2}v_t(x,t)\phi_n(x)\,dx \\
&= \frac{1}{2R_aC_m}\int_0^\ell (a^2v_x)_x\phi_n\,dx - \frac{G_m}{C_m}\psi_n(t) \\
&= \frac{1}{2R_aC_m}\left\{a^2v_x\phi_n\Big|_0^\ell - \int_0^\ell v_xa^2\phi_n'\,dx\right\} - \frac{G_m}{C_m}\psi_n(t) \\
&= \frac{i_0(t)\phi_n(0)}{2C_m\pi} + \frac{1}{2R_aC_m}\int_0^\ell (a^2\phi_n')'v\,dx - \frac{G_m}{C_m}\psi_n(t) \\
&= \frac{i_0(t)\phi_n(0)}{2C_m\pi} - \frac{\mu_n}{2R_aC_m}\psi_n(t) - \frac{G_m}{C_m}\psi_n(t) \\
&= \frac{i_0(t)\phi_n(0)}{2C_m\pi} - \lambda_n\psi_n(t)
\end{aligned}$$

where

$$\lambda_n \equiv \frac{\mu_n + 2R_aG_m}{2R_aC_m}. \tag{2.13}$$

It follows that ψ_n must satisfy

$$\psi_n'(t) + \lambda_n\psi_n(t) = \frac{i_0(t)\phi_n(0)}{2C_m\pi} \tag{2.14}$$

while (2.4) requires, in addition, that

$$\psi_n(0) = 0. \tag{2.15}$$

The solution to (2.14)–(2.15) is

$$\psi_n(t) = \frac{\phi_n(0)}{2C_m\pi}\int_0^t \exp(\lambda_n(r-t))i_0(r)\,dr.$$

Inserting this into (2.7) we find

$$v(x,t) = \frac{1}{2C_m\pi}\sum_{n=0}^\infty \phi_n(0)\phi_n(x)\int_0^t \exp(\lambda_n(r-t))i_0(r)\,dr. \tag{2.16}$$

From here it is a simple matter to compute the Laplace transform

$$\begin{aligned}
\hat{v}(x,s) &= \int_0^\infty \exp(-st)v(x,t)\,dt \\
&= \frac{1}{2C_m\pi}\sum_{n=0}^\infty \phi_n(0)\phi_n(x)\int_0^\infty \exp(-(s+\lambda_n)t)\int_0^t \exp(\lambda_nr)i_0(r)\,dr\,dt \\
&= \frac{\hat{i}_0(s)}{2C_m\pi}\sum_{n=0}^\infty \frac{\phi_n(0)\phi_n(x)}{s+\lambda_n}
\end{aligned} \tag{2.17}$$

and arrive at the input impedance, i.e., the ratio of the Laplace transforms of the input potential and current,

$$z(s) \equiv \frac{\hat{v}(0,s)}{\hat{i}_0(s)} = \frac{1}{2C_m\pi}\sum_{n=0}^{\infty}\frac{\phi_n^2(0)}{s+\lambda_n}. \tag{2.18}$$

We record its first two derivatives

$$z'(s) = -\frac{1}{2C_m\pi}\sum_{n=0}^{\infty}\frac{\phi_n^2(0)}{(s+\lambda_n)^2} \quad \text{and} \quad z''(s) = \frac{1}{C_m\pi}\sum_{n=0}^{\infty}\frac{\phi_n^2(0)}{(s+\lambda_n)^3}$$

and find, at $s=0$, that

$$z(0) = \frac{R_a}{\pi}\sum_{n=0}^{\infty}\frac{\phi_n^2(0)}{\mu_n+q} \tag{2.19}$$

$$z'(0) = \frac{-2R_a^2C_m}{\pi}\sum_{n=0}^{\infty}\frac{\phi_n^2(0)}{(\mu_n+q)^2} \tag{2.20}$$

$$z''(0) = \frac{8R_a^3C_m^2}{\pi}\sum_{n=0}^{\infty}\frac{\phi_n^2(0)}{(\mu_n+q)^3} \tag{2.21}$$

where

$$q \equiv 2R_aG_m. \tag{2.22}$$

As a result, the particular combination

$$\frac{z(0)z''(0)}{(z'(0))^2} = 2\frac{\sum_{n=0}^{\infty}\frac{\phi_n^2(0)}{\mu_n+q}\sum_{n=0}^{\infty}\frac{\phi_n^2(0)}{(\mu_n+q)^3}}{\left(\sum_{n=0}^{\infty}\frac{\phi_n^2(0)}{(\mu_n+q)^2}\right)^2} \equiv F(q) \tag{2.23}$$

is an equation in the single unknown, q. In practice we have found that F is monotone over the range of physiologically reasonable q and hence measurement of $F(q)$ uniquely determines q. That $F(q)$ can indeed be measured follows from the fact, recall Cox [4], that z and its derivatives at $s=0$ may be expressed in terms of low order moments of the input current and potential. More precisely, if

$$M_n(f) \equiv \int_0^{\infty} t^n f(t)\,dt$$

denotes the nth moment of f and $v_0(t) \equiv v(0,t)$ then

$$\begin{aligned} z(0) &= \frac{M_0(v_0)}{M_0(i_0)} \\ z'(0) &= \frac{M_0(v_0)M_1(i_0) - M_0(i_0)M_1(v_0)}{M_0^2(i_0)} \\ z''(0) &= \frac{M_2(v_0)M_0(i_0) - M_2(i_0)M_0(v_0) - 2M_1(v_0)M_1(i_0) + 2M_1^2(i_0)z(0)}{M_0^2(i_0)}. \end{aligned} \tag{2.24}$$

Once q is determined from (2.23) it is a simple matter to recover each of the desired passive parameters. More precisely, one need only follow the

Single Potential Algorithm

I. Inject $i_0(t)$, record $v_0(t)$ and compute $\{M_j(i_0)\}_{j=0}^2$ and $\{M_j(v_0)\}_{j=0}^2$.
II. Compute $z(0)$, $z'(0)$, and $z''(0)$ per (2.24).
III. Solve (2.23) for q.
IV. Substitute $z(0)$ and q in (2.19) and solve for R_a.
V. Substitute q and R_a in (2.22) and solve for G_m.
VI. Substitute $z'(0)$, q and R_a in (2.20) and solve for C_m.

Of course steps III–VI require the solution of (2.8)–(2.9). As mentioned above this only requires knowledge of the fiber length, ℓ, and taper $a(x)$ – data that is readily acquired via staining and light microscopy following step I.

Let us immediately put this algorithm to the test. We consider a fiber for which

$$\begin{aligned} &\ell = 0.1\ cm,\ R_a = 0.03\ k\Omega cm,\ C_m = 1\ \mu F/cm^2,\ G_m = 0.3\ mS/cm^2, \\ &a(x) = \exp(-10x)/1000\ cm,\ i_0(t) = t\exp(-t)/300\ \mu A. \end{aligned} \tag{2.25}$$

In order to determine $v_0(t)$ we solved (2.3)–(2.6) via finite elements in space, step size of $2\ \mu m$, and finite differences in time, step size of $5\ \mu s$. See the Appendix for details of the implementation. The resulting input potential is plotted in figure 1.

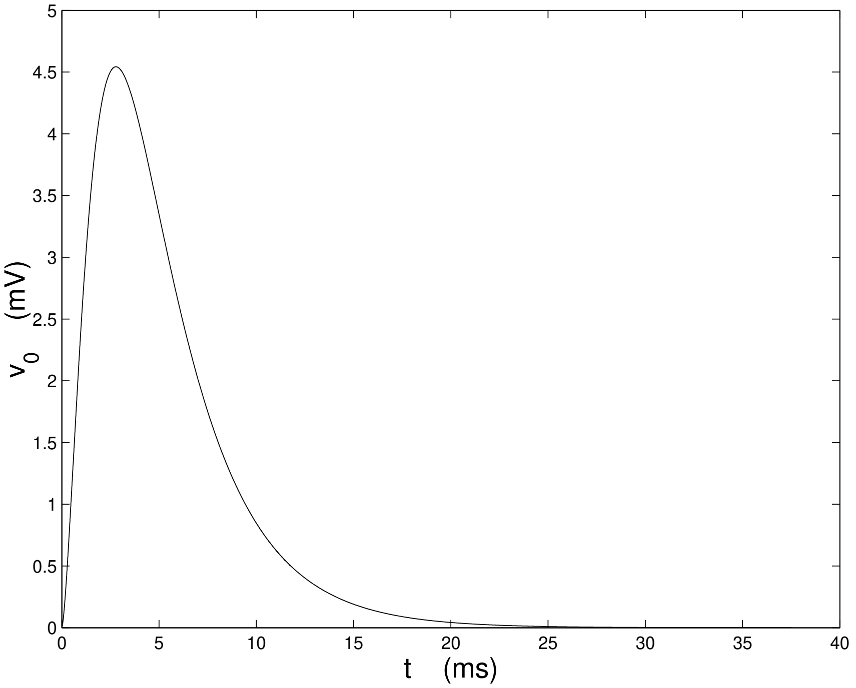

Figure 1. The input potential for the fiber and current source specified in (2.25).

With i_0 and v_0 we may carry out steps I and II and arrive at the value

$$F(q) = \frac{z(0)z''(0)}{(z'(0))^2} = 2.0892 \tag{2.26}$$

In using (2.23) to determine q we must address the error involved in truncating the three sums. Discretizing the eigenvalue problem, (2.8)–(2.9), via the aforementioned choice of finite elements produces tridiagonal stiffness and mass matrices of size 501×501. We have used Matlab's `eigs` function to compute the eigenpairs $\{(\mu_n, \phi_n)\}_{n=0}^{500}$, normalized and ordered as specified in (2.11)–(2.10). Recalling the standard Sturm–Liouville oscillation theory we note that ϕ_N ought to have precisely N zeros. As our computed ϕ_N is not identically zero but is defined at only 501 points it follows that it can not have more than 250 zeros. Hence, roughly speaking, the computed pairs $\{(\mu_n, \phi_n)\}_{n=250}^{500}$ can not be accurate. We hope therefore to be able to safely truncate the three sums in (2.23) well before their 250th terms. As an indication that this is indeed safe we plot in figure 2A the value of

$$F_N(q) \equiv 2\frac{\sum_{n=0}^{N} \frac{\phi_n^2(0)}{\mu_n+q} \sum_{n=0}^{N} \frac{\phi_n^2(0)}{(\mu_n+q)^3}}{\left(\sum_{n=0}^{N} \frac{\phi_n^2(0)}{(\mu_n+q)^2}\right)^2} \tag{2.27}$$

as a function of N at $q = 0.018$.

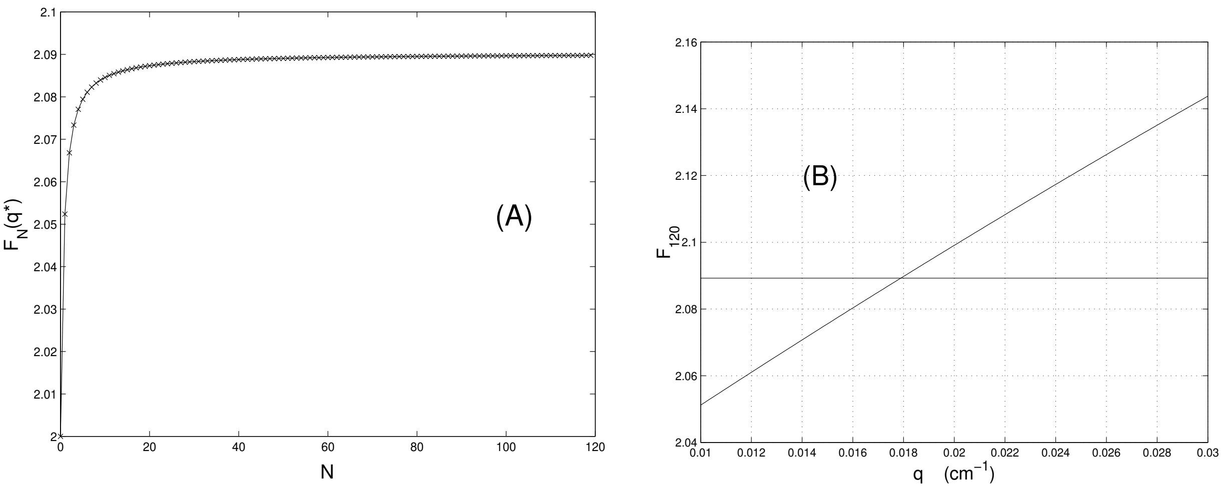

Figure 2. (A) The role of truncation in the evaluation of F. (B) Recovery of q from $F_{120}(q)$. The horizontal line is the measured value of $F(q)$ from (2.26). The diagonal line is the value of $F_{120}(q)$ from (2.27) as q varies between 0.01 and 0.03.

From (2.25) we find that the exact value of q, call it q^e, is 0.018. From figure 2B the graphs intersect just short of q^e at the recovered value $q^r \approx 0.01789$. Using this value in step IV we estimate R_a to be $R_a^r = 0.0298$. Using these values in steps V and VI produces $G_m^r = 0.0299$ and $C_m^r = 0.9988$. Each of these recovered values is indeed accurate to within 1%. In order to be of practical use, our algorithm must demonstrate some insensitivity to errors in the recorded geometry and potential. We note that errors in the measurement of the fiber length, ℓ, and radius, $a(x)$, will lead to errors in the spectral data, $\{\mu_n, \phi_n^2(0)\}_{n=0}^{N}$, computed from (2.8)–(2.9), and that these errors will taint the computation of the right hand side of (2.23). For example, if the resolution of the neuron tracing apparatus is 1 μm then the true radius is replaced with the step function depicted in figure 3.

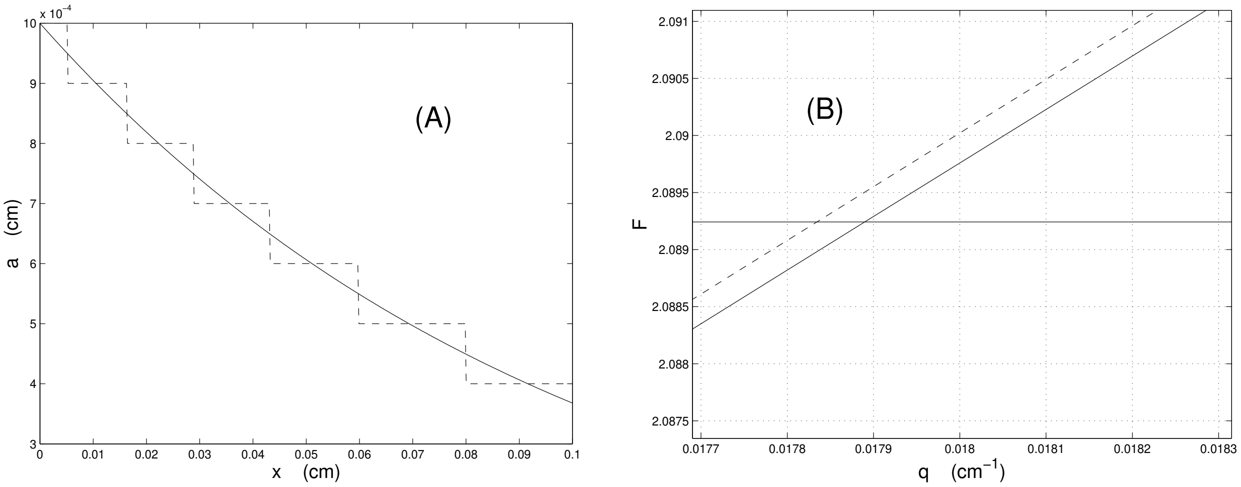

Figure 3.(A) The solid curve is the true radius, given in (2.25). The dashed curve is the 'measured' radius. (B) The solid diagonal is the graph of F_{120} using the true radius. The dashed diagonal is the graph of F_{120} using the step–wise measured radius.

From figure 3B we see that the effect of the crude measurement of a upon F is quite small. More precisely, the graph of F now crosses the value set by (2.26) at $q^r \approx 0.01783$. This value then engenders $R_a^r = 0.0297$, $G_m^r = 0.2998$ and $C_m^r = 0.9985$, still within 1% of true.

While errors in anatomical quantities produce errors in the computed graph of F, errors in measured input potential produce errors in the moments and therefore error in the value of $F(q)$ as determined in (2.26). For example, if we round each value of the computed v_0, as depicted in figure 1, to the closest 1/100th of a millivolt then the value of 2.0892 computed for the untainted v_0 becomes 2.0709. With regard to figure 4, the graph of F, whether for true or tainted a, crosses 2.0709 at $q^r \approx 0.014$ and so we find $R_a^r = 0.0236$, $G_m^r = 0.2971$ and $C_m^r = 0.9776$. Though the latter two are respectable we see that R_a^r is off by more than 20%.

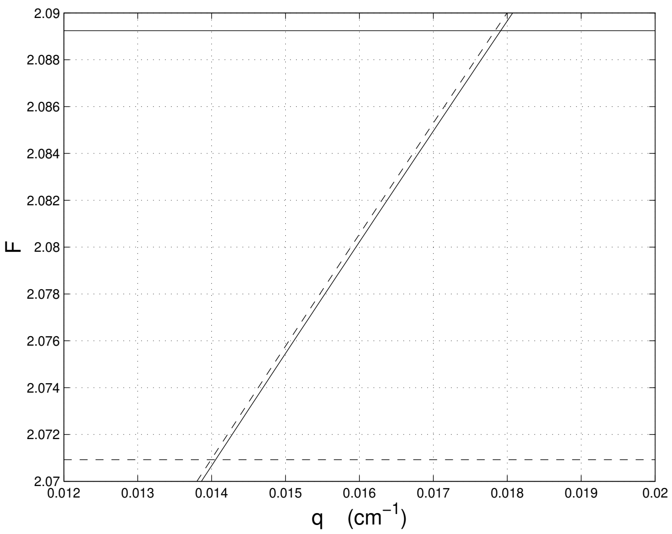

Figure 4. The effect of errors in a **and** v_0. The solid (dashed) diagonal is the graph of F_{120} using the clean (rounded) a. The solid (dashed) horizontal line is the level of $F(q)$ using the clean (rounded) v_0.

This large error in q and therefore R_a stems from the large errors in higher moments of v_0 stemming from the (fairly mild) rounding of its exponential tail. One can of course fit the decaying part of the measured v_0 to an exponential and hence re-attach an estimate of its true tail and so improve the accuracy of the moments. In addition, one can argue that with additional voltage measurements higher moments are in fact not required to recover the desired passive parameters. Let us flesh out that last remark.

We suppose that we may simultaneously measure both end potentials during excitation by a known current stimulus at $x = 0$. We ask then what do v_0 and $v_\ell \equiv v(\ell, t)$ tell us about R_a, G_m and C_m. As in Cox and Griffith [7] we turn to the transfer function

$$T(s) \equiv \frac{\hat{v}_\ell(s)}{\hat{v}_0(s)}. \tag{2.28}$$

Recalling (2.13) and (2.17) we find

$$T(s) = \frac{\sum_{n=0}^{\infty} \phi_n(0)\phi_n(\ell)/(2R_aC_m s + \mu_n + q)}{\sum_{n=0}^{\infty} \phi_n^2(0)/(2R_aC_m s + \mu_n + q)} \tag{2.29}$$

From here it is obvious that $T(0)$ depends only on q. As $T(0)$ is nothing more than the ratio of the integral of v_ℓ and v_0 it follows that

$$\frac{M_0(v_\ell)}{M_0(v_0)} = \frac{\sum_{n=0}^{\infty} \phi_n(0)\phi_n(\ell)/(\mu_n + q)}{\sum_{n=0}^{\infty} \phi_n^2(0)/(\mu_n + q)} \equiv H(q) \tag{2.30}$$

determines q. With q in hand one recovers R_a, G_m and C_m as above. The advantage then of a second potential recording is that we need only moments up to the first order. The precise procedure is expressed in the

Dual Potential Algorithm

I. Inject $i_0(t)$, record $v_0(t)$ and $v_\ell(t)$ and compute $\{M_j(i_0)\}_{j=0}^1$, $\{M_j(v_0)\}_{j=0}^1$ and $M_0(v_\ell)$.
II. Compute $z(0)$ and $z'(0)$ per (2.24).
III. Solve (2.30) for q.
IV. Substitute $z(0)$ and q in (2.19) and solve for R_a.
V. Substitute q and R_a in (2.22) and solve for G_m.
VI. Substitute $z'(0)$, q and R_a in (2.20) and solve for C_m.

We now compare the performance of this algorithm with the single potential version on the fiber and stimulus specified in (2.25). The two end potentials plotted in figure 5 reflect attenuation due to passive filtering.

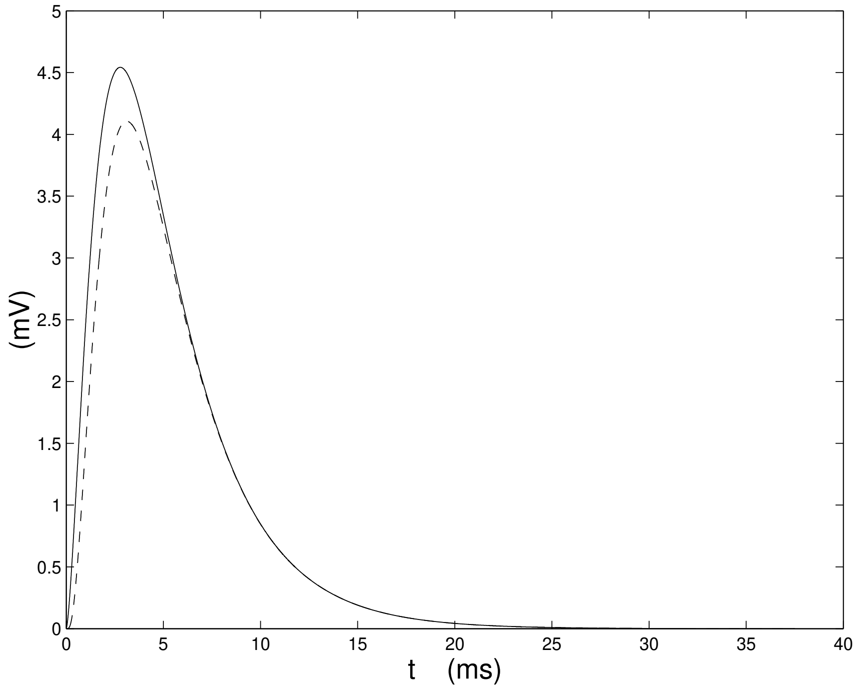

Figure 5. The input potential, v_0 (solid), and the end potential, v_ℓ (dashed) associated with the fiber and source of (2.25).

Step III of the dual potential algorithm now asks that we solve (2.30) for q. As with F we must, in practice, truncate the sums in the H defined by (2.30).

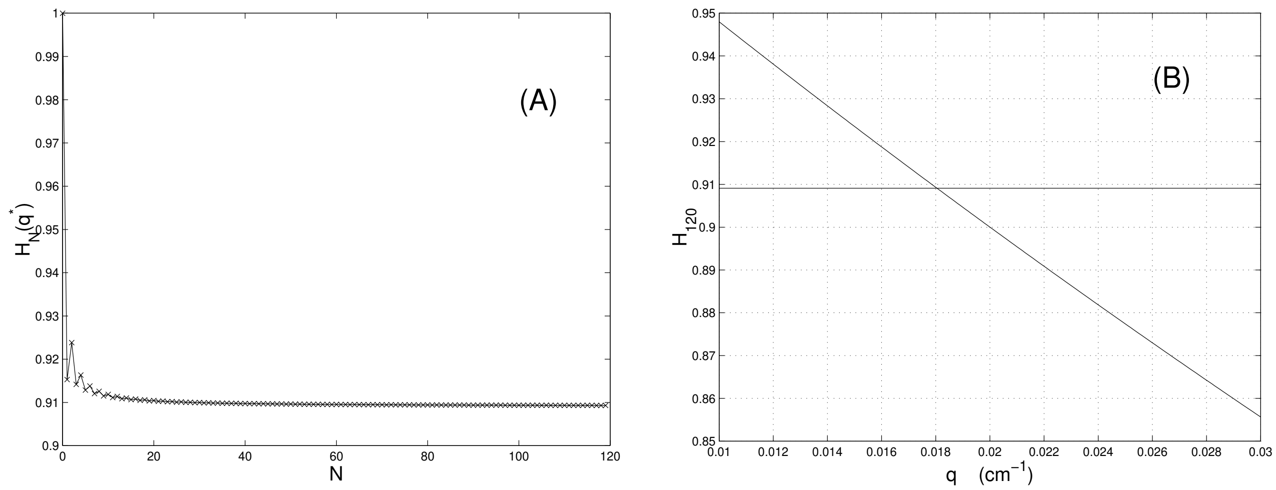

Figure 6. (A) The effect of truncation in (2.30) at the true, $q^* = 0.018$, value of q. H_N is the value of H when the two sums are truncated at the Nth term. (B) The diagonal line is the graph of $H_{120}(q)$. The horizontal line is the measured value of $T(0)$, i.e., $M_0(v_\ell)/M_0(v_0)$.

Figure 6B corresponds to step III of the algorithm and, as expected, determines the desired value of q. As above we next round the morphology, a, and potential recordings, v_0 and v_ℓ and apply the algorithm. As the dual potential algorithm relies on lower order moments we expect it to be more tolerant of noise in the potentials. We therefore continue to round a to the nearest micron but now round both v_0 and v_ℓ to the nearest **tenth** of a millivolt.

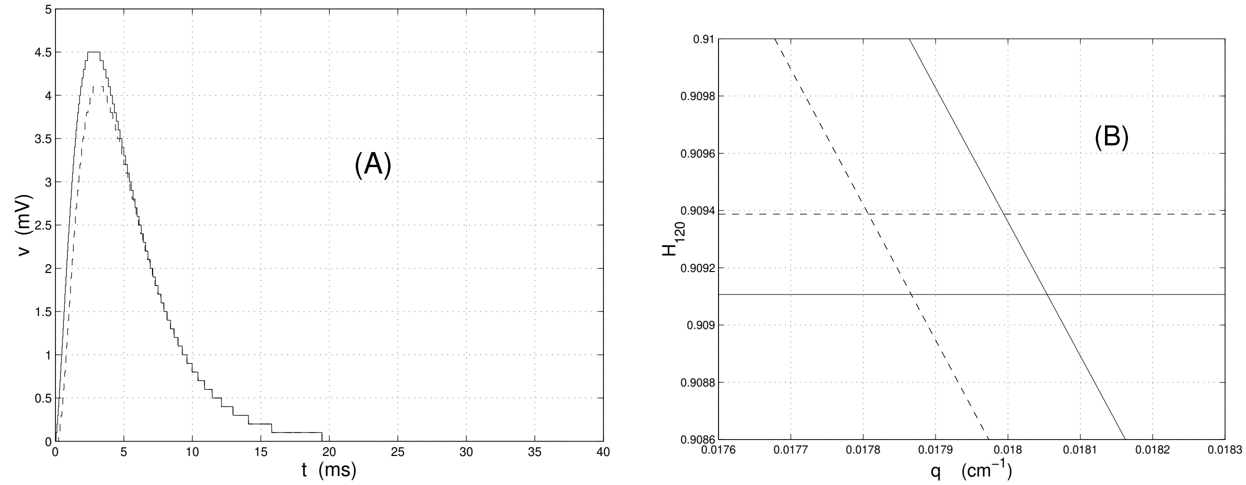

Figure 7. (A) The end potentials of figure 5 rounded to the nearest tenth of a millivolt. (B) The solid (dashed) diagonal is the graph of H using the clean (rounded) a. The solid (dashed) horizontal line is the value of $T(0)$ corresponding to clean (rounded) potentials.

The dashed lines in figure 7(B) intersect at $q^r \approx 0.01781$. This value, when used in the remaining steps, produces the highly accurate $R_a^r = 0.0296$, $G_m^r = 0.3004$ and $C_m^r = 0.9773$. In comparison we see that the double measurement results, with potentials corrupted by as much as $0.05\ mV$, are as accurate as the full precision single measurement results stemming from figure 3.

3. The Tapered Fiber with Soma

We now append to the left end of the fiber a soma with surface area A_s. We suppose that the soma membrane capacitance is that of the fiber, i.e., C_m, but permit the soma and fiber membrane conductances to differ. Denoting the soma membrane conductance by G_s and balancing currents at $x = 0$ we arrive at

$$\frac{\pi a^2(0)}{R_a} v_x(0,t) = A_s(C_m v_t(0,t) + G_s v(0,t)) - i_0(t), \tag{3.1}$$

in place of (2.5). These conditions of course coincide as $A_s \to 0$. Our interest is in showing how knowledge of v at $x = 0$ and $x = \ell$ leads to the effective determination of R_a, G_m, C_m and G_s. We begin, as in the previous section, by expanding v solely in terms of anatomical eigenfunctions. More precisely, we develop

$$v(x,t) = \sum_{n=0}^{\infty} \psi_n(t)\phi_n(x)$$

where, in keeping with (3.1), we ask the ϕ_n to satisfy

$$-(a^2\phi_n')' = \mu_n a\sqrt{1+(a')^2}\phi_n \tag{3.2}$$

$$\frac{2\pi}{A_s} a^2(0)\phi_n'(0) + (\mu_n + \gamma)\phi_n(0) = 0 \tag{3.3}$$

$$\phi_n'(\ell) = 0 \tag{3.4}$$

where

$$\gamma = 2R_a(G_m - G_s). \tag{3.5}$$

The effect of the soma is two-fold, the appearance of the eigenvalue parameter, μ_n, and the conductance mismatch parameter, γ, in (3.3), the boundary condition at $x = 0$. We shall argue below that both of these obstacles are benign.

First, although Tuckwell [19] laments the lack of an inner product with respect to which these eigenfunctions are orthogonal, such eigenvalue problems have received considerable attention since at least the work of Walter [20]. In particular, it is not hard to show that

$$\langle f, g\rangle \equiv \frac{A_s}{2\pi} f(0)g(0) + \int_0^\ell a\sqrt{1+(a')^2} fg\, dx. \tag{3.6}$$

will suffice. As such we may suppose that

$$\langle \phi_m, \phi_n\rangle = \delta_{mn} \tag{3.7}$$

and so find, as in (2.12), that

$$\psi_n(t) = \langle v(\cdot,t), \phi_n\rangle = \frac{A_s}{2\pi} v(0,t)\phi_n(0) + \int_0^\ell a(x)\sqrt{1+(a')^2} v(x,t)\phi_n(x)\, dx.$$

Although its differentiation in t proceeds in theory much like that of the previous section, in practice the calculation exposes exactly how the eigenfunction boundary condition, (3.3), accommodates the actual soma condition, (3.1). To wit,

$$\begin{aligned}
\psi_n'(t) &= \frac{A_s}{2\pi} v_t(0,t)\phi_n(0) + \int_0^\ell a\sqrt{1+(a')^2} v_t(x,t)\phi_n(x)\, dx \\
&= \frac{1}{2\pi C_m}\left(\frac{\pi a^2(0)}{R_a} v_x(0,t) - A_s G_s v(0,t) + i_0(t)\right)\phi_n(0) \\
&\quad + \frac{1}{2R_a C_m}\int_0^\ell ((a^2 v_x)_x - qa\sqrt{1+(a')^2} v)\phi_n(x)\, dx \\
&= \frac{1}{2\pi C_m}\left(\frac{\pi a^2(0)}{R_a} v_x(0,t) - A_s G_s v(0,t) + i_0(t)\right)\phi_n(0) \\
&\quad + \frac{a^2(0)\phi_n'(0)v(0,t) - \phi_n(0)a^2(0)v_x(0,t)}{2R_a C_m} \\
&\quad - \frac{\mu_n + q}{2R_a C_m}\int_0^\ell a\sqrt{1+(a')^2} v\phi_n\, dx \\
&= \frac{1}{2\pi C_m}\left(-A_s G_s v(0,t) + i_0(t)\right)\phi_n(0) - \frac{\mu_n + \gamma}{2R_a C_m}\frac{A_s}{2\pi} v(0,t)\phi_n(0) \\
&\quad - \frac{\mu_n + q}{2R_a C_m}\int_0^\ell a\sqrt{1+(a')^2} v\phi_n\, dx \\
&= \frac{i_0(t)\phi_n(0)}{2\pi C_m} - \frac{\mu_n + q}{2R_a G_m}\left\{\frac{A_s}{2\pi} v(0,t)\phi_n(0) + \int_0^\ell a\sqrt{1+(a')^2} v\phi_n\, dx\right\} \\
&= \frac{i_0(t)\phi_n(0)}{2\pi C_m} - \lambda_n\psi_n(t)
\end{aligned}$$

exactly as in the previous section, and hence

$$v(x,t) = \frac{1}{2\pi C_m} \sum_{n=0}^{\infty} \phi_n(0)\phi_n(x) \int_0^t \exp(\lambda_n(r-t)) i_0(r)\, dr$$

where λ_n remains as in (2.13). It follows that $\hat{v}$ remains (2.17) and the transfer function is precisely (2.29) and (2.30), the only rub being that the μ_n and ϕ_n now depend on γ through (3.3). Although this can not be avoided we can establish

Proposition 1. *The transfer function, $T(s)$, is independent of the shunt conductance G_s.*

Proof: We note that $\hat{v}$ satisfies the boundary value problem

$$\begin{aligned}
(a^2 \hat{v}_x)_x &= \mu^2(s) a \sqrt{1+(a')^2}\, \hat{v} \\
\pi a_1^2(0) \hat{v}_x(0,s) &= R_a A_s (C_m s + G_s) \hat{v}(0,s) - R_a \hat{i}_0(s) \\
\hat{v}_x(\ell, s) &= 0
\end{aligned}$$

where $\mu(s) = \sqrt{2R_a(C_m s + G_m)}$. As such we may represent $\hat{v}$ via

$$\hat{v}(x,s) = b_1(s) w_1(x,s) + b_2(s) w_2(x,s)$$

where w_1 and w_2 are solutions of the initial value problems (prime denotes d/dx)

$$(a^2 w_j')' = \mu^2(s) a \sqrt{1+(a')^2}\, w_j \tag{3.8}$$

$$w_1(0,s) = 1, \quad w_1'(0,s) = 0 \tag{3.9}$$

$$w_2(0,s) = 0, \quad w_2'(0,s) = 1, \tag{3.10}$$

and b_1 and b_2 are chosen to satisfy the boundary conditions on $\hat{v}$. In particular, $\hat{v}_x(\ell, s) = 0$ requires that

$$b_2(s) = -b_1(s) w_1'(\ell, s) / w_2'(\ell, s) \tag{3.11}$$

and so

$$\hat{v}(x,s) = b_1(s) \{ w_1(x,s) - w_1'(\ell,s) w_2(x,s) / w_2'(\ell,s) \} \tag{3.12}$$

so long as $w_2'(\ell,s) \neq 0$. If $w_2'(\ell,s) = 0$ then $\mu^2(s)$ would be an eigenvalue of

$$\begin{aligned}
(a^2 y')' &= \omega a \sqrt{1+(a')^2}\, y \\
y(0) &= y'(\ell) = 0.
\end{aligned}$$

This problem however has no positive eigenvalues. Hence (3.12) has sense and so may be used to write

$$T(s) = \frac{\hat{v}(\ell,s)}{\hat{v}(0,s)} = \frac{w_1(\ell,s) - w_1'(\ell,s) w_2(\ell,s)/w_2'(\ell,s)}{w_1(0,s) - w_1'(\ell,s) w_2(0,s)/w_2'(\ell,s)}.$$

We conclude the proof by noting that, via (3.8)–(3.10), both w_1 and w_2 are independent of G_s. ∎

The upshot of this proposition is that, so far as T is concerned, G_s may just as well be G_m. Applying this observation to (3.2)–(3.4) permits us to set $\gamma = 0$ and therefore arrive at a purely anatomical eigenvalue problem. To help make this clear, let us denote the eigenvalues and eigenfunctions of (3.2)–(3.4) by $\mu_n(\gamma)$ and $\phi_n(x,\gamma)$. It follows that the analog of (2.30),

$$\frac{M_0(v_\ell)}{M_0(v_0)} = \frac{\sum_{n=0}^\infty \phi_n(0,0)\phi_n(\ell,0)/(\mu_n(0)+q)}{\sum_{n=0}^\infty \phi_n^2(0,0)/(\mu_n(0)+q)} \equiv H(q) \tag{3.13}$$

may be solved for q. As the input impedance, z, however is not independent of G_s, we may not proceed to deduce R_a from (2.19). Rather, we continue to exploit T's freedom from G_s and note that (2.29) yields

$$T'(0) = -2R_aC_m \frac{\sum_{n=0}^\infty \frac{\phi_n^2(0,0)}{\mu_n(0)+q} \sum_{n=0}^\infty \frac{\phi_n(0,0)\phi_n(\ell,0)}{(\mu_n(0)+q)^2} - \sum_{n=0}^\infty \frac{\phi_n(0,0)\phi_n(\ell,0)}{\mu_n(0)+q} \sum_{n=0}^\infty \frac{\phi_n^2(0,0)}{(\mu_n(0)+q)^2}}{\left(\sum_{n=0}^\infty \phi_n^2(0,0)/(\mu_n(0)+q)\right)^2} \tag{3.14}$$

while elementary properties of the Laplace Transform yield

$$T'(0) = \frac{M_0(v_0)M_1(v_\ell) - M_1(v_0)M_0(v_\ell)}{M_0^2(v_0)}. \tag{3.15}$$

With q in hand these two expressions together determine R_aC_m. With q and R_aC_m we may now determine the actual value of γ from the logarithmic derivative at $s=0$ of the input impedance. More precisely, as

$$z(s) = \frac{R_a}{\pi}\sum_{n=0}^\infty \frac{\phi_n^2(0,\gamma)}{2R_aC_ms + \mu_n(\gamma) + q} \tag{3.16}$$

if $\Psi(s) \equiv (\log z(s))'$ then

$$\Psi(0) = \frac{z'(0)}{z(0)} = -2R_aC_m \frac{\sum_{n=0}^\infty \frac{\phi_n^2(0,\gamma)}{(\mu_n(\gamma)+q)^2}}{\sum_{n=0}^\infty \frac{\phi_n^2(0,\gamma)}{\mu_n(\gamma)+q}} \equiv P(\gamma) \tag{3.17}$$

while, in terms of moments

$$\Psi(0) = \frac{M_1(i_0)}{M_0(i_0)} - \frac{M_1(v_0)}{M_0(v_0)}. \tag{3.18}$$

As γ is the only unknown in (3.17) we find that (3.17)–(3.18) determine γ. With γ in hand we may return to (3.16) and finally determine R_a. From, R_a, $2R_aG_m$, $2R_aC_m$ and $2R_a(G_m - G_s)$ it is a simple matter to pick off G_m, C_m and G_s. We summarize our findings in the

Dual Potential Algorithm, with soma

I. Inject $i_0(t)$, record $v_0(t)$ and $v_\ell(t)$ and compute $\{M_j(i_0),\, M_j(v_0),\, M_j(v_\ell)\}_{j=0}^{1}$.
II. Solve (3.13) for q.
III. Use (3.14) to evaluate $2R_aC_m$.
IV. Solve (3.17) for γ.
V. Set $s=0$ in (3.16) and evaluate R_a.
VI. From R_a, $2R_aG_m$, $2R_aC_m$ and $2R_a(G_m-G_s)$ evaluate G_m, C_m and G_s.

We now exercise this algorithm on the fiber and source in (2.25) with a soma of surface area and membrane conductance

$$A_s = 24\times 10^{-6}\ cm^2, \qquad G_s = 0.6\ mS/cm^2, \tag{3.19}$$

respectively. We solve the corresponding initial–boundary value problem, (2.3),(2.4),(2.6) and (3.1), via finite elements in space and finite differences in time as described in the previous section and detailed in the Appendix. Comparing figure 5 and 8 we note the attenuating effect of the soma.

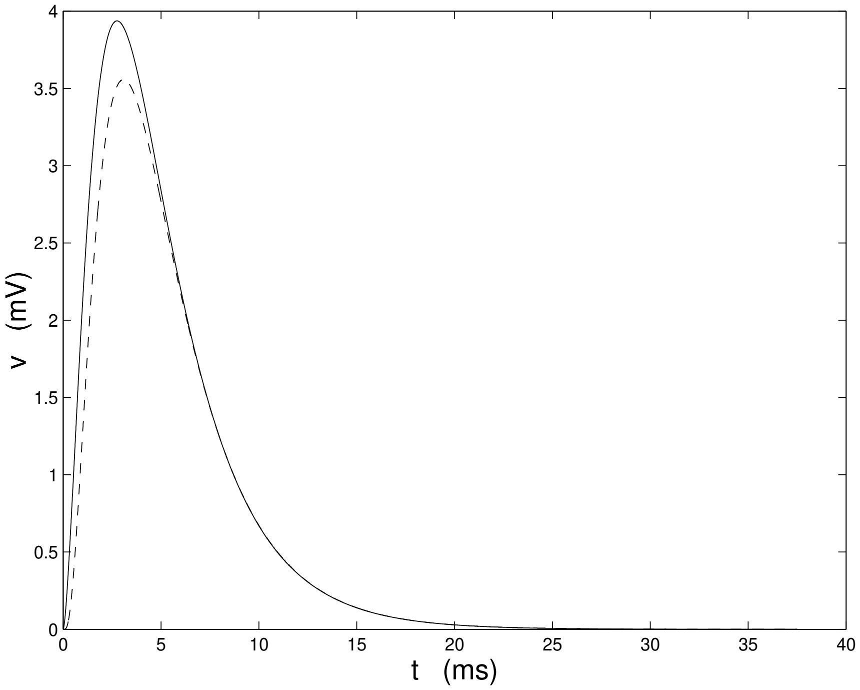

Figure 8. The input potential, v_0 (solid), and the end potential, v_ℓ (dashed) associated with the fiber and source of (2.25) and soma of (3.19).

Using the two potentials of figure 8 we visualize steps II and IV, with and without noise, in figure 9. The noise is created by rounding the values of a to the nearest micron and the values of v_0 and v_ℓ to the nearest tenth of a millivolt. We have, as in the previous section, found it safe to incorporate but the first 120 terms in each of sums comprising H and P.

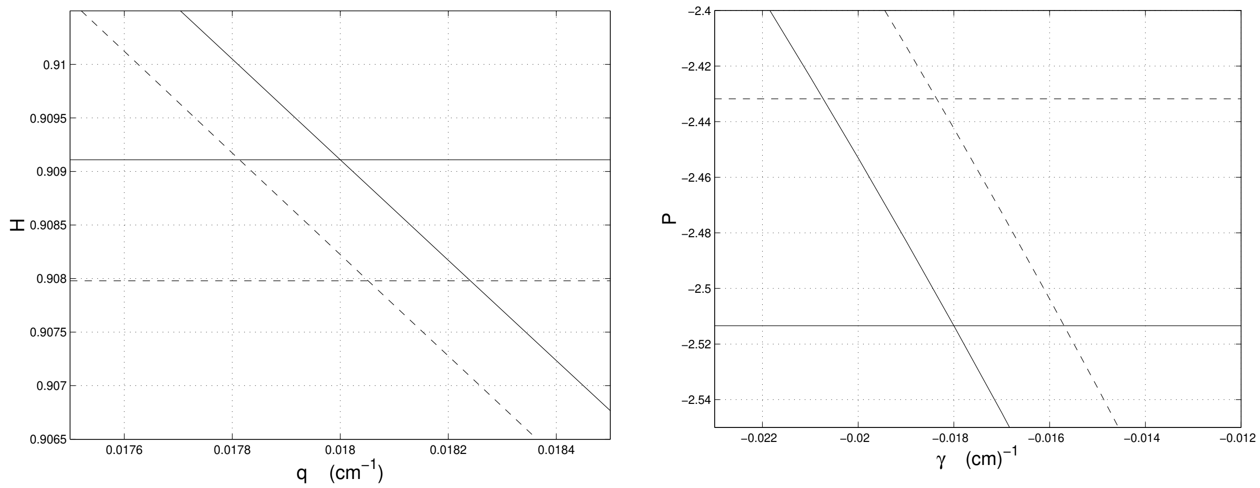

Figure 9. (A) The solid (dashed) diagonal line is the graph of H using the clean (rounded) a. The horizontal solid (dashed) line is the value of the lefthand side in (3.13) using the clean (rounded) potentials. The dashed lines intersect at $q^r \approx 0.01805$ which, when used in step III produces $(2R_aC_m)^r \approx 0.05843$. (B) The solid diagonal line is the graph of P for the unrounded a and exact values of q and $2R_aC_m$. The dashed diagonal line is the graph of P for the rounded a and the q^r and $(2R_aC_m)^r$ recovered from panel (A). The horizontal solid (dashed) line is the value of $\Psi(0)$ in (3.18) using the clean (rounded) potentials.

We deduced from figure 9(A) that $q^r \approx 0.01805$ and then from (3.14) that $(2R_aC_m)^r \approx 0.05843$. These values lead to the P of figure 9(B) from which we read $\gamma^r \approx -0.01836$ which in turn allows us to conclude that the recovered parameters

$$R_a^r \approx 0.0301 \quad G_m^r \approx 0.3001 \quad C_m^r \approx 0.9712 \quad \text{and} \quad G_s^r \approx 0.6053$$

all lie within 3% of their true values. This is surprising given the large errors in the measured potentials. The explanation that jumps from figure 9 is that errors in the geometry compensate for errors in the potentials, in the sense that the dashed lines cross at roughly the same abscissas as the solid lines. This sounds unlikely to be true in nature. Hence, the parallelograms in figure 9 should be taken as the region of 'reasonable' crossings. Taking the extreme (lower right) vertex in each case, as opposed to the fortuitous vertex above, still produces the quite reasonable

$$R_a^r \approx 0.0291 \quad G_m^r \approx 0.3139 \quad C_m^r \approx 1.0066 \quad \text{and} \quad G_s^r \approx 0.5706.$$

These results would most likely be improved by smoothing the corrupted a, v_0 and v_ℓ.

4. **Branched Neurons with Soma**

We now consider dendritic neurons with B branches and S splittings, or branch points. The branch index of the parent at the kth branch point is p_k while the branch indices of the two children are c_k^1 and c_k^2. A child that is not a parent will be called a leaf. We use $\mathcal{L}$ to denote the set of leaf indices. The radius and length of branch b are a_b and ℓ_b, respectively, each in cm. The membrane potential on the bth branch, $v_b(x,t)$, satisfies (2.3), i.e.,

$$\frac{1}{2R_a}\partial_x(a_b^2\partial_x v_b) = a_b\sqrt{1+(a_b')^2}(C_m\partial_t v_b + G_m v_b), \qquad b=0,\ldots,B-1. \tag{4.1}$$

At each branch point, we enforce continuity of potential and conservation of current via

$$v_{p_k}(\ell_{p_k},t) = v_{c_k^1}(0,t) = v_{c_k^2}(0,t), \tag{4.2}$$
$$a_{p_k}^2(\ell_{p_k})\partial_x v_{p_k}(\ell_{p_k},t) = a_{c_k^1}^2(0)\partial_x v_{c_k^1}(0,t) + a_{c_k^2}^2(0)\partial_x v_{c_k^2}(0,t). \tag{4.3}$$

Finally, assuming current stimulus at the soma and seals at the distal ends of the leaves, we arrive at

$$\frac{\pi a_0^2(0)}{R_a}\partial_x v_0(0,t) = A_s(C_m\partial_t v_0(0,t) + G_s v_0(0,t)) - i_0(t), \tag{4.4}$$
$$\partial_x v_b(\ell_b,t) = 0, \qquad b\in\mathcal{L}. \tag{4.5}$$

We note that (4.1)–(4.5) is not the most general model. We have only permitted 2 children per parent, one apical trunk, and no basal tree. All of these may be accommodated in what follows without changing the theory or algorithm.

We gather the branch potential in the vector of functions

$$V = [v_0\ v_2\ \cdots\ v_{B-1}] \tag{4.6}$$

and, as in previous sections, expand

$$V(x,t) = \sum_{n=0}^{\infty}\psi_n(t)\Phi_n(x) \tag{4.7}$$

where Φ_n is now the vector–valued eigenfunction

$$\Phi_n(x) = [\phi_{n,0}(x)\ \phi_{n,2}(x)\ \cdots\ \phi_{n,B-1}(x)]$$

whose elements obey

$$\begin{aligned}
-(a_b^2\phi_{n,b}')' &= \mu_n a_b\sqrt{1+(a_b')^2}\phi_{n,b}\\
\phi_{n,p_k}(\ell_{p_k}) &= \phi_{n,c_k^1}(0) = \phi_{n,c_k^2}(0),\\
a_{p_k}^2(\ell_{p_k})\phi_{n,p_k}'(\ell_{p_k}) &= a_{c_k^1}^2(0)\phi_{n,c_k^1}'(0) + a_{c_k^2}^2(0)\phi_{n,c_k^2}'(0)\\
\phi_{n,b}'(\ell_b) &= 0, \qquad b\in\mathcal{L}\\
\frac{2\pi}{A_s}a_0^2(0)\phi_{n,0}'(0) &+ (\mu_n+\gamma)\phi_{n,0}(0) = 0
\end{aligned} \tag{4.8}$$

where $\gamma = 2R_a(G_m - G_s)$ as before. This falls within the purview of problems studied by von Below [21] and it is not difficult to show that

$$\langle f, g\rangle \equiv \frac{A_s}{2\pi} f_0(0)g_0(0) + \sum_{b=0}^{B-1} \int_0^{\ell_b} a_b\sqrt{1+(a_b')^2} f_b g_b \, dx \tag{4.9}$$

is the inner product for which

$$\langle \Phi_m, \Phi_n\rangle = \delta_{mn}$$

and so $\psi_n(t) = \langle V(\cdot, t), \Phi_n\rangle$ and so (4.7) takes the form

$$V(x,t) = \frac{1}{2\pi C_m} \sum_{n=0}^{\infty} \phi_{n,0}(0)\Phi_n(x) \int_0^t \exp(\lambda_n(r-t)) i_0(r)\, dr \tag{4.10}$$

with, λ_n, as always as found in (2.13). Recording potential at the soma and out in the dendrite at point x_d on the dth branch provides

$$v_0(t) \equiv v_0(0,t) \quad \text{and} \quad v_d(t) \equiv v_d(x_d, t).$$

Arguing from (4.10) as in the previous section we may prove that the transfer function, i.e., the ratio of the Laplace transforms of v_d to v_0 is independent of G_s. This permits us to (provisionally) set $\gamma = 0$ in (4.8) and so find (compare (3.13))

$$\frac{M_0(v_d)}{M_0(v_0)} = \frac{\sum_{n=0}^{\infty} \phi_{n,0}(0,0)\phi_{n,d}(x_d,0)/(\mu_n(0)+q)}{\sum_{n=0}^{\infty} \phi_{n,0}^2(0,0)/(\mu_n(0)+q)} \equiv H(q). \tag{4.11}$$

We solve this for q and then, as in (3.14) and (3.15), conclude that

$$\begin{aligned}\frac{M_0(v_0)M_1(v_d) - M_1(v_0)M_0(v_d)}{2R_aC_mM_0^2(v_0)} &= \frac{\sum_{n=0}^{\infty} \frac{\phi_{n,0}(0,0)\phi_{n,d}(x_d,0)}{\mu_n(0)+q} \sum_{n=0}^{\infty} \frac{\phi_{n,0}^2(0,0)}{(\mu_n(0)+q)^2}}{\left(\sum_{n=0}^{\infty} \phi_{n,0}^2(0,0)/(\mu_n(0)+q)\right)^2} \\ &\quad - \frac{\sum_{n=0}^{\infty} \frac{\phi_{n,0}(0,0)\phi_{n,d}(x_d,0)}{(\mu_n(0)+q)^2}}{\sum_{n=0}^{\infty} \phi_{n,0}^2(0,0)/(\mu_n(0)+q)}\end{aligned} \tag{4.12}$$

and so determine $2R_aC_m$. As in (3.16)–(3.18) we arrive at the following equation for γ,

$$\Psi(0) = \frac{M_1(i_0)}{M_0(i_0)} - \frac{M_1(v_0)}{M_0(v_0)} = -2R_aC_m \frac{\sum_{n=0}^{\infty} \frac{\phi_{n,0}^2(0,\gamma)}{(\mu_n(\gamma)+q)^2}}{\sum_{n=0}^{\infty} \frac{\phi_{n,0}^2(0,\gamma)}{\mu_n(\gamma)+q}} \equiv P(\gamma). \tag{4.13}$$

With q and γ one then recovers R_a from

$$\frac{M_0(v_0)}{M_0(i_0)} = \frac{R_a}{\pi} \sum_{n=0}^{\infty} \frac{\phi_{n,0}^2(0,\gamma)}{\mu_n(\gamma)+q} \tag{4.14}$$

The final algorithm then differs very little from that of the previous section. Namely,

Dual Potential Algorithm, branched neuron with soma

I. Inject $i_0(t)$, record $v_0(t)$ and $v_d(t)$ and compute $\{M_j(i_0),\, M_j(v_0),\, M_j(v_d)\}_{j=0}^{1}$.

II. Solve (4.11) for q.

III. Use (4.12) to evaluate $2R_aC_m$.

IV. Solve (4.13) for γ.

V. Use (4.14) to evaluate R_a.

VI. From R_a, $2R_aG_m$, $2R_aC_m$ and $2R_a(G_m - G_s)$ evaluate G_m, C_m and G_s.

We now exercise this algorithm on the tapered wishbone of figure 10, with recordings taken at the soma and the distal end of branch 2.

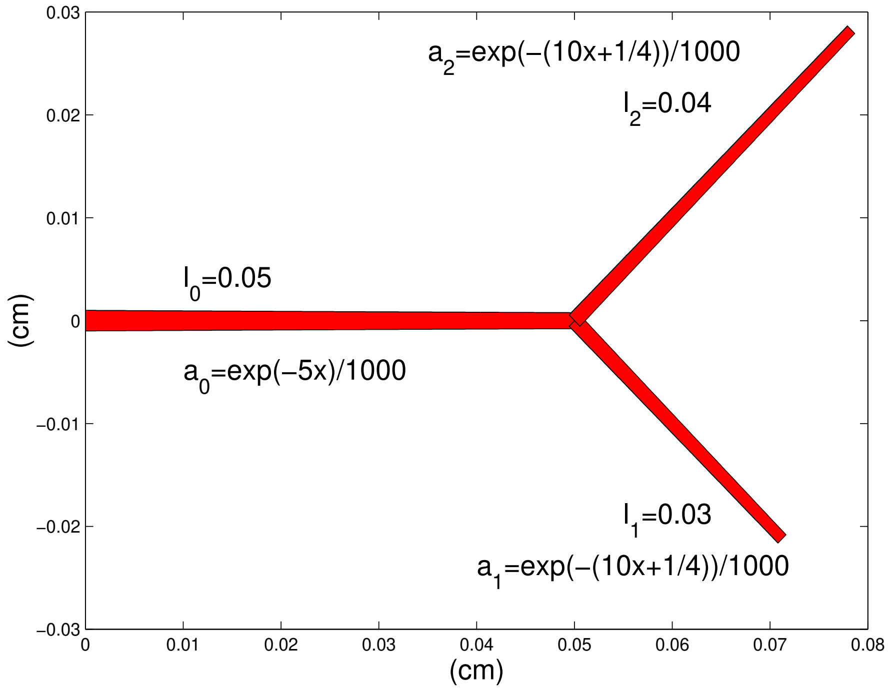

Figure 10. A tapered neuron with three branches, lengths and radii as specified.

The current stimulus, electrical parameters and soma area remain those stated in (2.25) and (3.19). As above, our spatial step is $h = 2\mu m$, our time step is $\tau = 5\mu s$ for 7500 steps, and we truncate all sums involving eigenvalues at the 120th term. The computed potentials at the soma and distal end of branch 2 are plotted below.

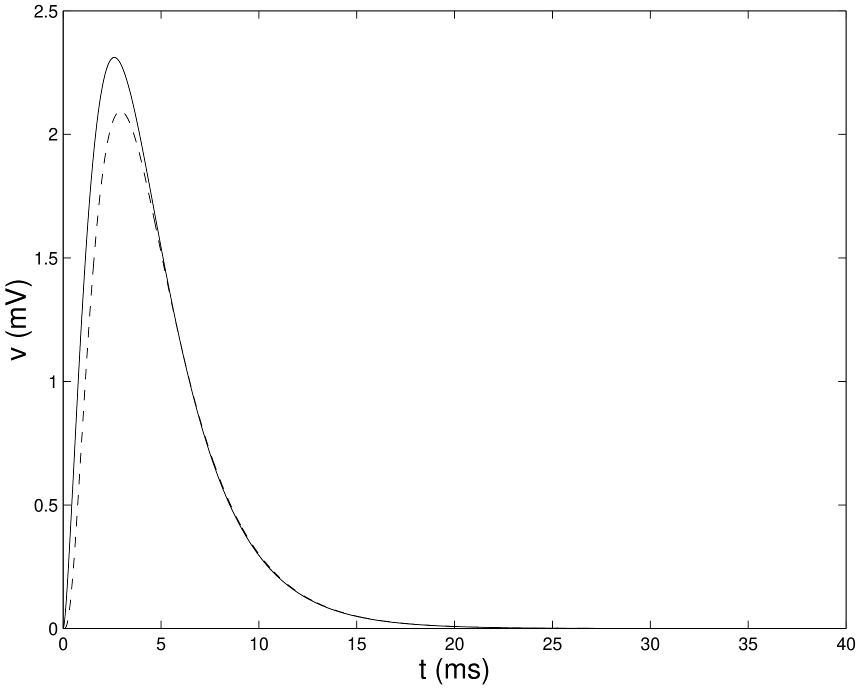

Figure 11. Computed v_0 (solid) and v_d (dashed) for the neuron of fig. 10.

We now graph the associated H and P functions and their experimentally derived values, in the pristine and rounded states. The rounding is precisely as above, each a_b to the nearest micron and v_0 and v_d to the nearest tenth of a millivolt.

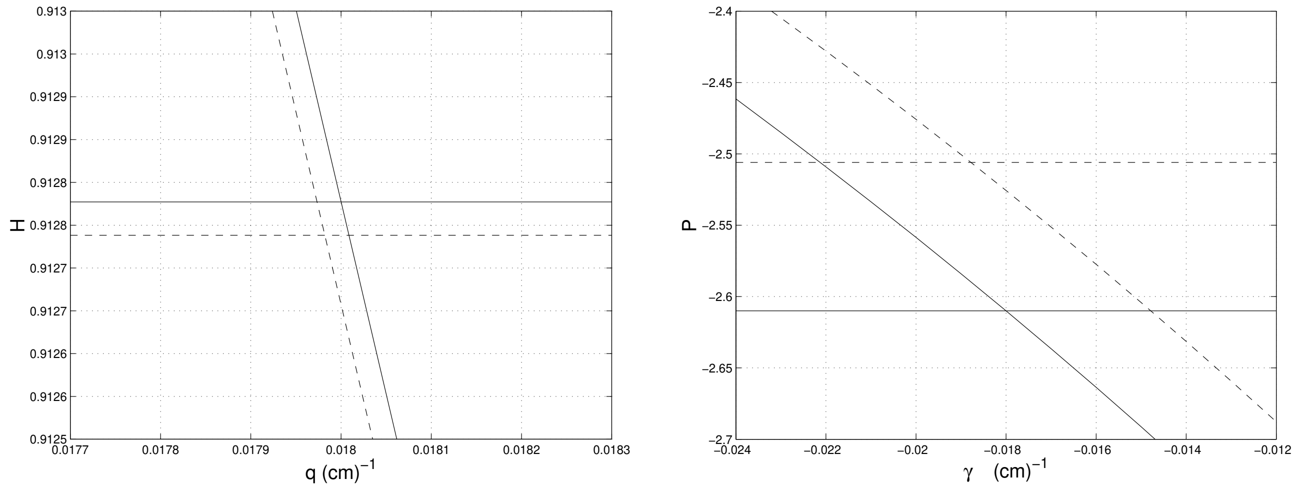

Figure 12. (A) The solid (dashed) diagonal line is the graph of H using the clean (rounded) radii. The horizontal solid (dashed) line is the value of the lefthand side in (4.11) using the clean (rounded) potentials. The dashed lines intersect at $q^r \approx 0.01799$ which, when used in step III produces $(2R_aC_m)^r \approx 0.05801$. (B) The solid diagonal line is the graph of P for the clean radii and exact values of q and $2R_aC_m$. The dashed diagonal line is the graph of P for the rounded radii and the q^r and $(2R_aC_m)^r$ recovered from panel (A). The horizontal solid (dashed) line is the value of $\Psi(0)$ in (4.13) using the clean (rounded) potentials.

We deduced from figure 12(A) that $q^r \approx 0.01799$ and $(2R_aC_m)^r \approx 0.05801$. These values lead to the P of figure 12(B) from which we read $\gamma^r \approx -0.01868$ which in turn allows us to conclude that the recovered parameters

$$R_a^r \approx 0.0301, \quad G_m^r \approx 0.2997, \quad C_m^r \approx 0.9666 \quad \text{and} \quad G_s^r \approx 0.6110$$

and so conclude that, even at its most general, the algorithm retains its robustness. Though simple to graph, these P and H functions hide, or rather, condense the neuron's spectral content. We close therefore with a few snapshots of the main players in our recovery algorithm. Namely, the eigenfunctions, Φ_n, in the expansion (4.7).

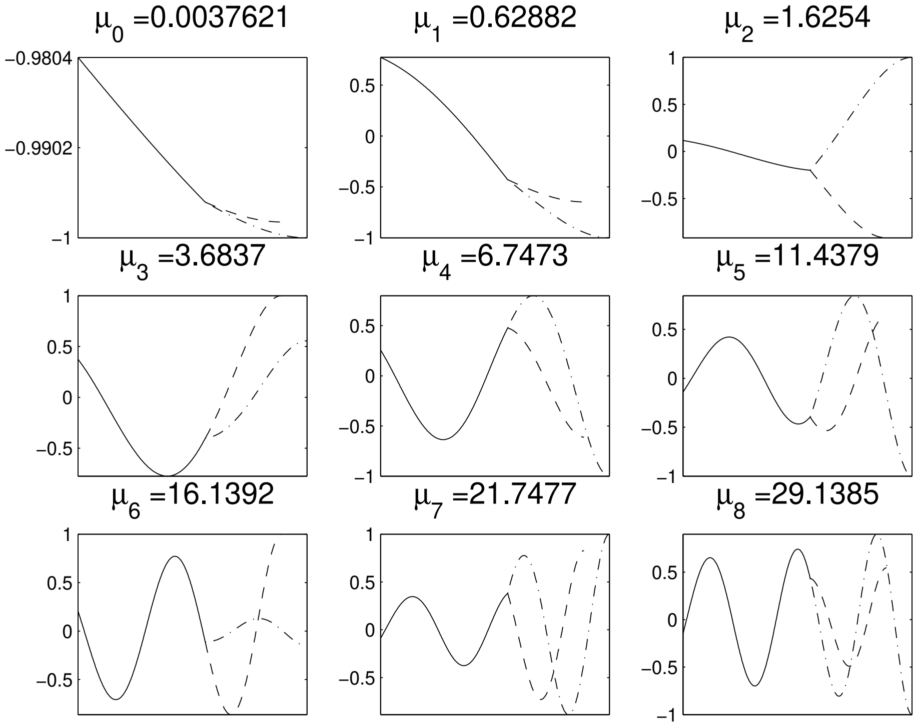

Figure 13. The first 9 eigenfunctions of the neuron in fig. 10. Above each panel is the associated eigenvalue μ_n. The solid curve is $\phi_{n,0}$, the dash–dot curve is $\phi_{n,1}$ and the dashed curve is $\phi_{n,2}$.

5. Appendix: Finite Element Methods for Tapered Cells

We construct finite difference in time, finite element in space discretizations of the equations for a branched neuron with soma by considering models of increasing generality.

The Tapered Fiber

Beginning with the equation for a single tapered fiber,

$$\frac{1}{2R_a}(a^2 v_x)_x = a\sqrt{1+(a')^2}(C_m v_t + G_m v) \tag{5.1}$$

we suppose that time comes in increments of τ and that functions of x may be written as linear combinations of shifted versions of the fundamental hat function,

$$T_0(x) \equiv \begin{cases} 1 - |x|/h & \text{if } |x| \le h \\ 0 & \text{otherwise} \end{cases}$$

More precisely, we write

$$v(x, j\tau) \approx v^{(j)}(x) \approx \sum_{i=0}^{N} v_i^{(j)} T_i(x) \quad \text{and} \quad a(x) \approx \sum_{i=0}^{N} a_i T_i(x)$$

where, if the fiber is of length ℓ then

$$N = \ell/h \quad \text{and} \quad T_i(x) = T_0(x - ih).$$

We replace the time derivative in (5.1) with a difference

$$\frac{1}{2R_a}(a^2 v_x^{(j)})_x = a\sqrt{1 + (a')^2}(C_m(v^{(j)} - v^{(j-1)})/\tau + G_m v^{(j)}) \tag{5.2}$$

We manage space by multiplying (5.2) across by T_k and integrating over the full length,

$$\begin{aligned} T_k(0)\frac{i_0^{(j)}}{2\pi} - \frac{1}{2R_a}\int_0^\ell a^2 v_x^{(j)} T_k' \, dx \\ = \int_0^\ell a\sqrt{1 + (a')^2}(C_m(v^{(j)} - v^{(j-1)})/\tau + G_m v^{(j)}) T_k \, dx \end{aligned} \tag{5.3}$$

We have integrated by parts and used the soma–less boundary conditions, (2.5)–(2.6). For fixed k, (5.3) is one linear equation in the $N+1$ unknowns, $\{v_i^{(j)}\}_{i=0}^N$. As k ranges from 0 to N we therefore recognize in (5.3) an $(N+1) \times (N+1)$ linear system for $v^{(j)}$. We proceed to the explicit calculation of the system matrices.

Beginning on the left side of the equality in (5.3), if $k = 0$,

$$\int_0^\ell a^2 v_x^{(j)} T_0' \, dx = \frac{(v_1^{(j)} - v_0^{(j)})(a_0^2 + a_1^2 + a_0 a_1)}{3h}$$

and similarly,

$$\int_0^\ell a^2 v_x^{(j)} T_N' \, dx = \frac{(v_N^{(j)} - v_{N-1}^{(j)})(a_{N-1}^2 + a_N^2 + a_N a_{N-1})}{3h}$$

while if $0 < k < N$ then

$$\begin{aligned} \int_0^\ell a^2 v_x^{(j)} T_k' \, dx = -v_{k+1}^{(j)} \frac{a_{k+1}^2 + a_k^2 + a_{k+1}a_k}{3h} - v_{k-1}^{(j)} \frac{a_{k-1}^2 + a_k^2 + a_{k-1}a_k}{3h} \\ + v_k^{(j)} \frac{a_{k-1}^2 + 2a_k^2 + a_{k+1}^2 + a_k(a_{k-1} + a_{k+1})}{3h} \end{aligned}$$

These three calculations contribute to the symmetric tridiagonal stiffness matrix K via

$$K_{k,k} = \frac{1}{3h}\begin{cases} a_0^2 + a_1^2 + a_0 a_1 & \text{if } k=0 \\ a_{k-1}^2 + 2a_k^2 + a_{k+1}^2 + a_k(a_{k-1}+a_{k+1}) & \text{if } 0<k<N \\ a_{N-1}^2 + a_N^2 + a_N a_{N-1} & \text{if } k=N \end{cases} \tag{5.4}$$
$$K_{k,k+1} = -\frac{a_{k+1}^2 + a_k^2 + a_{k+1}a_k}{3h} \qquad 0 \le k < N.$$

Note, that if a is in fact constant then $K = a^2 K_{\mathcal{N}}/h$ where $K_{\mathcal{N}}$ is the familiar Neumann finite difference matrix with twos on the diagonal (except for ones in the first and last places) and negative ones on the super and sub diagonals.

Turning now to the right side of the equality in (5.3), we find, when $k=0$,

$$\int_0^\ell a\sqrt{1+(a')^2}v^{(j)}T_0\,dx = \frac{\sqrt{h^2+(a_0-a_1)^2}}{12}\{v_1^{(j)}(a_1+a_0) + v_0^{(j)}(a_1+3a_0)\}$$

and similarly

$$\int_0^\ell a\sqrt{1+(a')^2}v^{(j)}T_N\,dx = \frac{\sqrt{h^2+(a_{N-1}-a_N)^2}}{12}\{v_{N-1}^{(j)}(a_{N-1}+a_N) + v_N^{(j)}(a_{N-1}+3a_N)\}$$

while if $0<k<N$ then

$$\begin{aligned}\int_0^\ell a\sqrt{1+(a')^2}v^{(j)}T_k\,dx &= v_{k+1}^{(j)}\sqrt{h^2+(a_k-a_{k+1})^2}(a_{k+1}+a_k)/12 \\ &+ v_{k-1}^{(j)}\sqrt{h^2+(a_k-a_{k-1})^2}(a_{k-1}+a_k)/12 \\ &+ v_k^{(j)}\big\{\sqrt{h^2+(a_k-a_{k-1})^2}(a_{k-1}+3a_k) + \sqrt{h^2+(a_k-a_{k+1})^2}(a_{k+1}+3a_k)\big\}/12\end{aligned}$$

We collect these three in the symmetric tridiagonal mass matrix

$$M_{k,k} = \frac{1}{12}\begin{cases} (a_1+3a_0)\sqrt{h^2+(a_0-a_1)^2}) & \text{if } k=0 \\ \sqrt{h^2+(a_k-a_{k-1})^2}(a_{k-1}+3a_k)+ \\ \quad \sqrt{h^2+(a_k-a_{k+1})^2}(a_{k+1}+3a_k) & \text{if } 0<k<N \\ (a_{N-1}+3a_N)\sqrt{h^2+(a_{N-1}-a_N)^2} & \text{if } k=N \end{cases} \tag{5.5}$$
$$M_{k,k+1} = \frac{\sqrt{h^2+(a_k-a_{k+1})^2}(a_{k+1}+a_k)}{12} \qquad 0 \le k < N.$$

With $e_0 = [1\ 0\ \cdots\ 0]^T$ we may now write (5.1) as

$$\frac{i_0^{(j)}}{2\pi}e_0 - \frac{1}{2R_a}Kv^{(j)} = (G_m + C_m/\tau)Mv^{(j)} - (C_m/\tau)Mv^{(j-1)}$$

or

$$(2R_a(G_m\tau + C_m)M + \tau K)v^{(j)} = 2R_aC_mMv^{(j-1)} + R_a\tau i_0^{(j)}e_0/\pi. \tag{5.6}$$

This is the linear system, implicit in (5.3), that one must solve in order to propagate potentials from the past, time $(j-1)\tau$, to the present, time $j\tau$. By the same token, the discretization of the associated Neumann eigenvalue (2.8)–(2.9) is

$$K\phi = \mu M\phi. \tag{5.7}$$

and the orthonormality relation, (2.11), is mirrored in

$$\phi_n^T M\phi_m = \delta_{mn}.$$

As discussed in §2 only the small amplitude eigenvalues of (5.7) are of any value. This contradicts the statement by Zador and Perlmutter in appendix 3 to Koch [22] that one is interested in the eigenvalues of large magnitude and that block power methods are therefore recommended. In order to compute the smallest 120 eigenvalues of (5.7) we use `eigs(K,M,120,'sm')`, the Matlab implementation of ARPACK, see Lehoucq *et al.* [23].

The Tapered Fiber with Soma

Having carefully set things up, very little has to change in order to account for a soma and branching. The soma changes (5.3) to

$$\begin{aligned} T_k(0)\{i_0^{(j)}/(2\pi) - A_s(C_m(v_0^{(j)} - v_0^{(j-1)})/\tau + G_s v_0^{(j)})\} - \frac{1}{2R_a}\int_0^\ell a^2 v_x^{(j)} T_k' \, dx \\ = \int_0^\ell a\sqrt{1+(a')^2}(C_m(v^{(j)} - v^{(j-1)})/\tau + G_m v^{(j)})T_k \, dx \end{aligned} \tag{5.8}$$

and so,

$$(2R_a(G_m\tau + C_m)M^s + \tau K^s)v^{(j)} = 2R_a C_m M^s v^{(j-1)} + R_a \tau i_0^{(j)} e_0/\pi. \tag{5.9}$$

where M^s and K^s differ from M and K only in the $(0,0)$ element. Namely,

$$M_{0,0}^s = M_{0,0} + A_s \quad \text{and} \quad K_{0,0}^s = K_{0,0} - A_s\gamma$$

where γ is defined in (3.5). So (5.9) propagates past to present, $K^s\phi = \mu M^s\phi$ approximates the eigenvalue problem (3.2)–(3.4) and the orthonormality relation (3.6)–(3.7) is retained in $\phi_n^T M^s \phi_m = \delta_{mn}$.

The Branched Neuron with Soma

The issue here is getting the branch point conditions right. By right we mean the introduction of a branch element that retains the selfadjoint structure of the original continuous problem. In order to minimize clutter we restrict ourselves to a neuron with 3 branches of lengths ℓ_0, ℓ_1 and ℓ_2, meeting at a common branch point, as per figure 10. We continue to assume that the free end of branch 0 sports a soma and that the free ends of the other branches are sealed. Time discretization produces the three branch equations

$$\frac{1}{2R_a}(a^2 v_b^{(j)'})' = a\sqrt{1+(a')^2}(C_m(v_b^{(j)} - v_b^{(j-1)})/\tau + G_m v_b^{(j)}) \tag{5.10}$$

We suppose, for convenience, that each of the branch lengths is an integer multiple of the spatial step size, h. That is,

$$N_b = \ell_b/h \qquad j = 0, 1, 2.$$

On the root branch, we use

$$T_{0,i}(x) = T_0(x - ih), \quad i = 0, \ldots, N_0 - 1$$

and on the remaining,

$$T_{b,i}(x) = T_0(x - ih), \quad i = 1, \ldots, N_b.$$

These are obvious choices that jibe with our previous remarks on unbranched fibers. At the branch point we certainly need an element that spans all three fibers. The natural choice is the branched hat

$$T_{0,N_0}(x) = \begin{cases} T_0(x - N_0 h) & \text{if } x \text{ lies on branch } 0 \\ T_0(x) & \text{if } x \text{ lies on branch } 1 \text{ or } 2. \end{cases}$$

Continuity of potential and radius is assured on expressing

$$v_0^{(j)}(x) \approx \sum_{i=0}^{N_0} v_{0,i}^{(j)} T_{0,i}(x) \quad \text{and} \quad a_0(x) \approx \sum_{i=0}^{N_0} a_{0,i} T_{0,i}(x)$$

on the root and

$$v_b^{(j)}(x) \approx \sum_{i=1}^{N_b} v_{b,i}^{(j)} T_{b,i}(x) \quad \text{and} \quad a_b(x) \approx \sum_{i=1}^{N_b} a_{b,i} T_{b,i}(x), \qquad b = 1, 2.$$

on the remaining branches. Hence, at each time step, the

$$N \equiv N_0 + N_1 + N_2 + 1$$

unknowns in (5.10) are (with the (j) superscript suppressed for legibility)

$$[v_{0,0} \; v_{0,1} \; \cdots \; v_{0,N_0} \; v_{1,1} \; v_{1,2} \; \cdots \; v_{1,N_1} \; v_{2,1} \; v_{2,2} \; \cdots \; v_{2,N_2}]$$

We obtain N linear equations in these N unknowns by multiplying each of the three equations in (5.10) by each of our N functions, integrating over the length of each branch, and summing. Of course all but one of our hats is supported on a single branch and so only one of the equations in (5.10) contributes and we arrive at expressions identical to those found in the unbranched case. If, however, we multiply (5.10) by the branched hat T_{0,N_0} and integrate we find

$$\begin{aligned} \frac{1}{2R_a} a_0^2(\ell_0) v_0^{(j)'}(\ell_0) &- \frac{1}{2R_a h} \int_{\ell_0 - h}^{\ell_0} a_0^2 v_0^{(j)'}\, dx \\ &= \int_{\ell_0 - h}^{\ell_0} a_0 \sqrt{1 + (a_0')^2} (C_m (v_0^{(j)} - v_0^{(j-1)})/\tau + G_m v_0^{(j)}) T_{0,N_0}\, dx \end{aligned} \tag{5.11}$$

on the root, and

$$-\frac{1}{2R_a}a_b^2(0)v_b^{(j)'}(0)+\frac{1}{2R_a h}\int_0^h a_b^2 v_b^{(j)'}\,dx$$
$$=\int_0^h a_b\sqrt{1+(a_b')^2}(C_m(v_b^{(j)}-v_b^{(j-1)})/\tau+G_m v_b^{(j)})T_{0,N_0}\,dx \tag{5.12}$$

on the other two branches. We now sum these three equations. On the left we find 3 integrals and three terms evaluated at the branch point. The sum of the three terms at the branch point is precisely zero, on account of the current balance equation, (4.3). Evaluating and summing the 3 integrals we arrive at

$$\frac{1}{2R_a 3h}\Big\{(v_{0,N_0-1}^{(j)}-v_{0,N_0}^{(j)})(a_{0,N_0-1}^2+a_{0,N_0}^2+a_{0,N_0-1}a_{0,N_0})+$$
$$(v_{1,1}^{(j)}-v_{0,N_0}^{(j)})(a_{0,N_0}^2+a_{1,1}^2+a_{1,1}a_{0,N_0})+$$
$$(v_{2,1}^{(j)}-v_{0,N_0}^{(j)})(a_{0,N_0}^2+a_{2,1}^2+a_{0,N_0}a_{2,1})\Big\}$$

This dictates that the N_0th equation has nonzeros in positions $N_0-1,\ N_0,\ N_0+1$ and N_0+1+N_1. The latter is the interesting one. It is our first deviation form the tridiagonal state and translates into

$$K_{N_0,N_0+1+N_1}=-\frac{a_{0,N_0}^2+a_{2,1}^2+a_{0,N_0}a_{2,1}}{3h}.$$

Turning now to the sum of the three integrals on the right in (5.12), we find

$$\int_{\ell_0-h}^{\ell_0} a_0\sqrt{1+(a_0')^2}v_0^{(j)}T_{0,N_0}\,dx+\sum_{b=1}^{2}\int_0^h a_b\sqrt{1+(a_b')^2}v_b^{(j)}T_{0,N_0}\,dx$$
$$=\frac{\sqrt{h^2+(a_{0,N_0-1}-a_{0,N_0})^2}}{12}\{v_{0,N_0-1}^{(j)}(a_{0,N_0-1}+a_{0,N_0})+v_{0,N_0}^{(j)}(a_{0,N_0-1}+3a_{0,N_0})\}$$
$$+\sum_{b=1}^{2}\frac{\sqrt{h^2+(a_{b,1}-a_{0,N_0})^2}}{12}\{v_{b,1}^{(j)}(a_{b,1}+a_{0,N_0})+v_{0,N_0}^{(j)}(a_{b,1}+3a_{0,N_0})\}$$

and so the mass matrix too is no longer tridiagonal. In particular,

$$M_{N_0,N_0+1+N_1}=\frac{\sqrt{h^2+(a_{2,1}-a_{0,N_0})^2}}{12}(a_{2,1}+a_{0,N_0})$$

Similarly, if we multiply (5.10) by $T_{2,1}$, integrate and sum we find that

$$K_{N_0+1+N_1,N_0}=K_{N_0,N_0+1+N_1}\quad\text{and}\quad M_{N_0+1+N_1,N_0}=M_{N_0,N_0+1+N_1},$$

i.e., the branch point does not destroy the symmetry in K or M. One accommodates the soma precisely as described in the previous subsection. The assembly of the final stiffness and mass matrices requires the concatenation of the tridiagonal branch matrices with one additional element (placed symmetrically) for each branch point. The resulting linear system and eigenproblem retain the exact same form as (5.6) and (5.7).

6. Acknowledgements

This work was partially supported by NSF Grant DMS–0077728 and was partially conducted at the University of Utah, thanks to Jim Keener's hospitality.

7. References

[1] N.J. Bannister & J. Larkman, Dendritic morphology of CA1 pyramidal neurones from the rat hippocampus: I. Branching Patterns, J. Comparative Neurol. 360 (1995) 150-160.
[2] W. Rall, R.E. Burke, W.R. Holmes, J.J.B. Jack, S.J. Redman and I. Segev, Matching dendritic neuron models to experimental data, Physiol. Reviews 172 (1992) S159–S186.
[3] M.C. Vanier and J.M. Bower, A comparative survey of automated parameter search methods for compartmental neural models, J. of Computational Neuroscience 7(2) (1999) 149–171.
[4] S.J. Cox, A new method for extracting cable parameters from input impe–dance data, Math. Biosci. 153 (1998) 1–12.
[5] S.J. Cox & L. Ji, Identification of the cable parameters in the somatic shunt model, Biological Cybernetics 83 (2000) 151–159.
[6] S.J. Cox & L. Ji, Discerning ionic currents and their kinetics from input impedance data, Bull. Math. Biol. 63(5) (2001) 909–932.
[7] S.J. Cox & B.E. Griffith, Recovering quasi–active properties of dendritic neurons from dual potential recordings, J. Comp. Neurosci., to appear.
[8] J.K Engelhardt, F.R. Morales & M.H. Chase, An alternative method for the analysis of neuron passive electrical data which uses integrals of voltage transients, J. Neuroscience Methods 81 (1998) 131–138.
[9] R.S. Eisenberg & R.T. Mathias, Structural analysis of electrical properties of cells and tissues, CRC Critical Rev. Bioengineering 4 (1980) 203–232.
[10] R.H. Adrian & W. Almers, Membrane capacity measurements on frog skeletal muscle in media of low ion content, J. Physiology 337 (1974) 573–605.
[11] J.J.B. Jack, D. Noble, & R.W. Tsien, Electrical Current Flow in Excitable Cells, Clarendon Press, Oxford, 1975.
[12] W. Rall, Core conductor theory and cable properties of neurons, in: E.R. Kandel, (Ed.), Handbook of Physiology, Vol. 1, APS, Bethesda, MD, 1977, pp. 39–77.
[13] W. Rall, Cable theory for dendritic neurons, in: C. Koch and I. Segev, (Eds.),Methods in Neuronal Modeling,MIT Press, Cambridge, 1989, pp. 9–62.
[14] W. Rall & H. Agmon–Snir, Cable theory for dendritic neurons, in: C. Koch and I. Segev, (Eds.), Methods in Neuronal Modeling, 2nd ed., MIT Press, Cambridge, MA,

1998, pp. 27–92.
[15] H. Agmon–Snir, A novel theoretical approach to the analysis of dendritic transients, Biophys. J. 69 (1995) 1633–1656.
[16] A.L. Hodgkin, Lord Adrian: Obituary, Nature 275 (1977) 31.
[17] G. Strang & G. Fix, An Analysis of the Finite Element Method, Wellesley-Cambridge Press, 1997.
[18] W. Rall, Theory of physiological properties of dendrites, Ann, NY Acad. Sci. 96 (1962) 1071–1092.
[19] H.C. Tuckwell, Introduction to theoretical neurobiology, Vol. I, Linear Cable Theory and Dendritic Structure, Cambridge University Press, Cambridge, 1988.
[20] J. Walter, Regular eigenvalue problems with eigenvalue parameter in the boundary conditions, Mathematische Zeitschrift 133 (1973) 301–312.
[21] J. von Below, Sturm–Liouville eigenvalue problems on networks, Math. Methods in the Appl. Sciences 10 (1988) 383–395.
[22] C. Koch, Biophysics of Computation, Oxford University Press, Oxford, 1998.
[23] R.B. Lehoucq, D.C. Sorensen & C. Yang, ARPACK Users' Guide: Solution of Large-Scale Eigenvalue Problems with Implicitly Restarted Arnoldi Methods, SIAM Publications, Philadelphia, 1998.